TIME-DOMAIN RESPONSE OF SIMPLE ELASTIC SYSTEMS TO SEISMIC MOTION: ERROR ASSESSMENT AND ENGINEERING IMPLICATIONS

R. Blázquez[1]

[1] *Professor of Geotechnical Engineering, Department of Civil Engineering and Construction, Universidad de Castilla-La Mancha, Ciudad Real .Spain*
Email: Rafael.Blazquez@uclm.es

ABSTRACT :

Time-stepping methods and/or direct evaluation of Duhamel's integral are being increasingly used in earthquake engineering to solve the equations of motion for discrete and continuous systems, due to affordable computational costs, applicability to linear and non linear oscillators and permanent growth of the world data base of earthquake acelerogramas. Yet, when applying the above methods, one must be aware that all integration schemes, regardless of their stability and convergence characteristics, act as digital recursive filters that distort unevenly the frequency content of the input, and this may result in a misleading response of the system. Furthermore, in practice, the initial conditions for the computation of the response, in the case of analog excitations that have lost the initial portion of motion, are unknown and assumed to be zero for calculation purposes. This assumption, rigorously speaking, is only valid for high-frequency systems, (e.g., rigid structures), and leads to unconservative designs for long-period systems if the initial condition effects are not properly taken into account.
In this paper a rational criterion is presented to rank the accuracy of various commonly used integration procedures for the dynamics of soil and/or structural systems. A few examples are shown to compare the performance of the methods and their sensitivity to the factors controlling the integration error, namely, the amplitude of the time step, the variation of the motion values between sampling points, and the dynamic properties of the vibrating system.
The above question is of primary interest for short-to-intermediate period elastic systems, which are governed by the transient phase of the seismic response. For long period systems, which are governed mainly by the free-vibration part of the response, the study clearly shows large magnifications of the computed "non resting" response spectra with respect to the conventional calculations.

KEYWORDS: Time-integration algorithms, linear oscillators, transfer functions, initial conditions, response spectra, long-period systems.

1. INTRODUCTION

The direct dynamic analysis of the seismic response of soil and structural systems has become a standard method of analysis in recent years, side by side with the advances in the computational tools and the remarkable increase in the strong-motion data base at worldwide level. Similarly, the processing techniques and the analysis of seismic records have experienced profound changes in the last two decades, with the progressive substitution of the old analog records by the new digital ones. Both matters of problems have in common the essential need to minimize the integration errors in the determination of the correct values of the ground motion and/or the system response to the seismic action.
Numerical integration in the time domain requires to solve a number of questions related to the stability, convergence and accuracy of the integration method. The choice of the optimal algorithm for evaluating a particular response quantity is not an easy task, and frequently a trial and error procedure is adopted, reducing the integration interval until an adequate degree of accuracy is achieved. This research focuses on how to evaluate rigorously the performance of any time integration scheme, on the basis of comparing the transfer functions of the algorithm, for a given kinematic magnitude, with the ones corresponding to the ideal integrator (computed exactly). This methodology permits to know in advance which regions of the traces of the motion will be wrongly enhanced by numerical integration and/or affected by processing noise.

Another aspect of the investigation concerns the influence of initial motions on the spectral response of long period systems. Non-zero initial motions may arise when the systems is already moving when a seismic event occurs or from evaluation of the earthquake response when a segment at the beginning of the input record is not available. The latter situation is typical of optical accelerograms, since a small portion of the accelerogram is always lost due to the fact that the response of the instrument below the prefixed level of sensitivity cannot be recorded.

In conventional response spectrum computations, the initial conditions are ignored and the analysis is carried out assuming that the system is initially at rest; that is, assuming zero initial conditions. This assumption is generally valid for rigid and intermediate systems, for which the free vibration part of the response is not predominant and "at rest initial conditions" can be reasonably justified. There is, however, a paucity of information on the consequences of ignoring the effects of initial conditions on the spectral analysis of long period systems, which are not well understood yet. The present research is responsive to this need.

2. ACCURACY OF QUADRATURE RULES APPLIED TO OSCILLATORY FUNCTIONS

Generally speaking, time integration algorithms are nothing else but linear combinations of the numerical data (base points, t_i, and function to be integrated, $x(t_i)$), derived from polynomial approximations of the function $x(t_i)$, either for equidistant points (Newton-Cotes methods) or for points located at non-equal time intervals (Gaussian quadrature methods). In this paper, we restrict the analysis to four well known integration methods of the first category, namely the trapezoidal, Simpson's, rectangle and mid-point rules, which are shown schematically in Fig. 1.

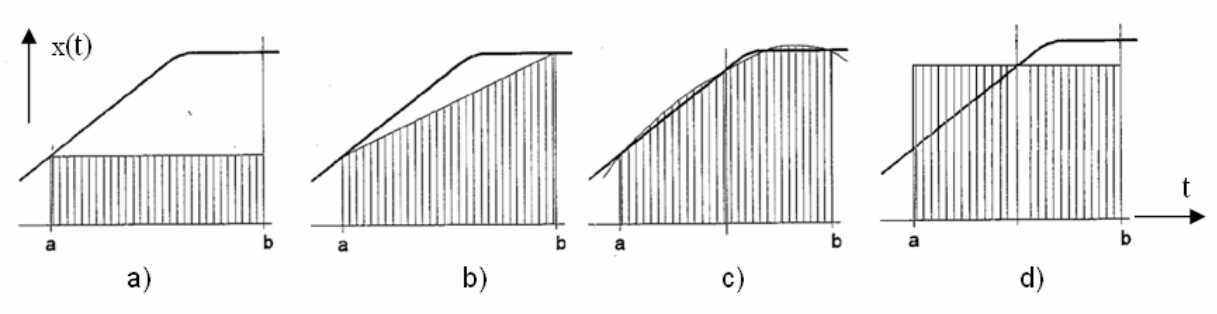

Figure 1.- Quadrature rules: a) rectangle; b) trapezoidal; c) Simpson's; d) mid-point

The mathematical formulation of these four methods is indicated in Table 2.1:

Table 2.1

Trapezoidal rule	**Simpson's rule**
$y_{n+1} = y_n + \frac{h}{2}(x_n + x_{n+1});\ n = 0,1,2,...$ (2.1)	$y_{n+1} = y_{n-1} + \frac{h}{3}(x_{n-1} + 4x_n + x_{n+1});\ n = 1,2,3...$ (2.2)
Rectangle rule	**Mid-point rule**
$y_{n+1} = y_n + hx_n;\ n = 0,1,2,...$ (2.3)	$y_{n+1} = y_n + hx_{n+1/2};\ n = 0,1,2,...$ (2.4)

where $h = t_j - t_i\ (j > i)$, and $y(t) = \int x(t)dt$ (2.5)

The integration schemes of Eqs. 2.1 - 2.4 can be characterized as recursive digital filters of causal type with memory. Therefore, according to Hamming (1977), their degree of accuracy for a given frequency can be estimated by computing the ratio between the transfer function of the numerical (approximate) and the analytical (exact) temporal operators. To do so, an input complex harmonic signal, $e^{i\omega t}$, is assumed. Since the above equations are all linear, the output signal after integration will be of the type $H(i\omega)e^{i\omega t}$, where $H(i\omega)$ is the complex transfer function of the integrator and ω is the angular frequency (Fig. 2).

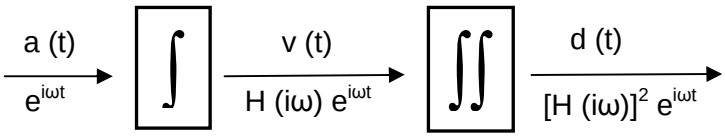

Figure 2.- Transfer functions of time integration operators applied to a seismic acceleration record

Then, for the ideal integrator it is found

$$H^*(i\omega)e^{i\omega t} = y(t) = \int e^{i\omega t}dt = \frac{e^{i\omega}}{i\omega} \qquad (2.6)$$

$$H^*(i\omega) = \frac{1}{i\omega}e^{-i\pi/2} \Rightarrow \left|H^*(i\omega)\right| = \frac{1}{\omega};\ \ \phi^*(i\omega) = -\frac{\pi}{2} \qquad (2.7)$$

whereas for the quadrature rules, making $x_n = e^{i\omega nh}$ and $y_n = H(i\omega)x_n$ in Eqs. 2.1-2.4, the expressions of Table 2.2 are derived (n=number of sampling points; h=Δt=discretization time interval).

Table 2.2

Trapezoidal rule	**Simpson's rule**
$H(i\omega) = \frac{h}{2}\cot(\frac{wh}{2})e^{-i\frac{\pi}{2}}$ (2.8)	$H(i\omega) = \frac{h}{3}\frac{2+\cos(\omega h)}{\sin(\omega h)}e^{-i\frac{\pi}{2}}$ (2.9)
Rectangle rule	**Mid-point rule**
$H(i\omega) = \frac{h}{2\cdot\sin(\frac{\omega h}{2})}e^{-i\left(\frac{\pi}{2}+\frac{\omega h}{2}\right)}$ (2.10)	$H(i\omega) = \frac{h}{2\cdot\sin(\frac{\omega h}{2})}e^{-i\frac{\pi}{2}}$ (2.11)

The moduli of the complex-variable functions 2.8 – 2.11, normalized with respect to that of the ideal integrator (Eqn. 2.7), are represented in Fig. 3-a, and the corresponding normalized phases angles are drawn in Fig. 3-b. In both diagrams $\omega_N=\pi/h$ is the so-called circular Nyquist frequency, which is the maximum frequency that can be reached if "aliasing" effects are to be avoided. From the inspection of Fig. 3, the following observations are made:

1) The rectangle, mid-point and Simpson's formulae amplify the amplitude of the signals throughout the whole frequency range (especially for harmonics above one-half of Nyquist frequency), whereas the trapezoidal rule attenuates progressively all the frequencies in the interval (0, ω_N).

2) The rectangle rule (also called "simple summation rule") is the only one that introduces a frequency-dependent phase shift in the integration process which leads to baseline drifts and distortions in the shape of the integrated signal (Fig. 3-b). Consequently, the use of the rectangle rule is not recommended for solving earthquake problems in engineering practice.

The practical implications of the above behavioral patterns are quite evident. Consider, for example, the simulated accelerogram proposed in the literature by Bogdanoff et al (1961)

$$\ddot{y}(t) = Bte^{\alpha t}\sum_{j=1}^{n}\cos(\omega_j t + \phi_j) \qquad (2.12)$$

with B=0.292 and α=-0.333; *n* is the number of harmonics with circular frequencies ω_j considered in the simulation, and Φ_j are random numbers uniformly distributed between 0 and 2π (Table 2.3).The artificial

accelerogram (2.12) is analytically integrable all the way up to the response spectra, thus permitting to calibrate very easily the effectiveness and accuracy of several integration methods currently employed in earthquake engineering. Besides, by choosing adequately the parameters *n* and ω_j , the frequency content of the signal can be controlled at will.

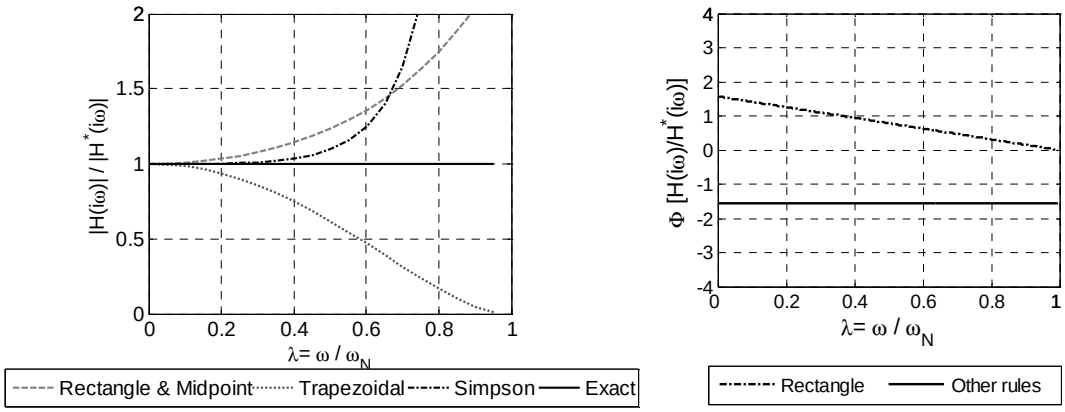

a) b)

Figure 3.- Normalized transfer functions of quadrature rules: a) amplitude values; b) phase angles

Table 2.3

ω_j (rad/sec)	6.00	8.00	10.00	11.15	12.30	13.25	14.15	16.20	17.35	19.15	22.00
ϕ_j (rad)	3.7663	1.3422	4.8253	0.2528	4.5204	1.8834	1.3320	1.7852	0.1517	2.4881	1.7654
ω_j (rad/sec)	25.25	29.85	34.50	39.60	46.45	53.00	58.60	66.75	71.15	74.80	80.25
ϕ_j (rad)	1.6632	2.1862	0.8325	1.2387	2.3156	3.0012	1.0645	0.7843	1.5532	0.9586	2.3562

Thus, Figure 4-a depicts the simulated accelerogram, for *n*= 22, and 6.00< ω_i < 80.25 rad/sec. On the other hand, in Fig. 4-b, *n*= 5, and 58.60< ω_i < 80.25 rad/sec. Integrating the accelerogram of Fig. 4-b by means of the Simpson's and trapezoidal rules, with h= 0.025 sec (40 sample points per second), gives the diagrams of Figs. 5-b and 5-c, while the exact velocigram is represented in Fig. 5-a. It becomes obvious how the trapezoidal rule truncates the high frequency peaks of the integrated signal whereas the Simpson's rule magnifies those peaks, an undesirable and deleterious effect if spurious noise due to poor processing of the signal is to be expected.

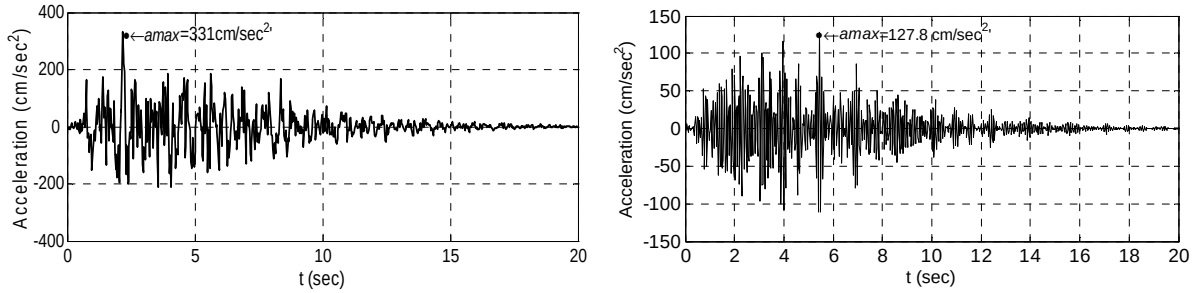

a) b)

Figure 4.-Simulated accelerograms (Bogdanoff et al, 1961): a) standard; b) enriched in high frequencies.

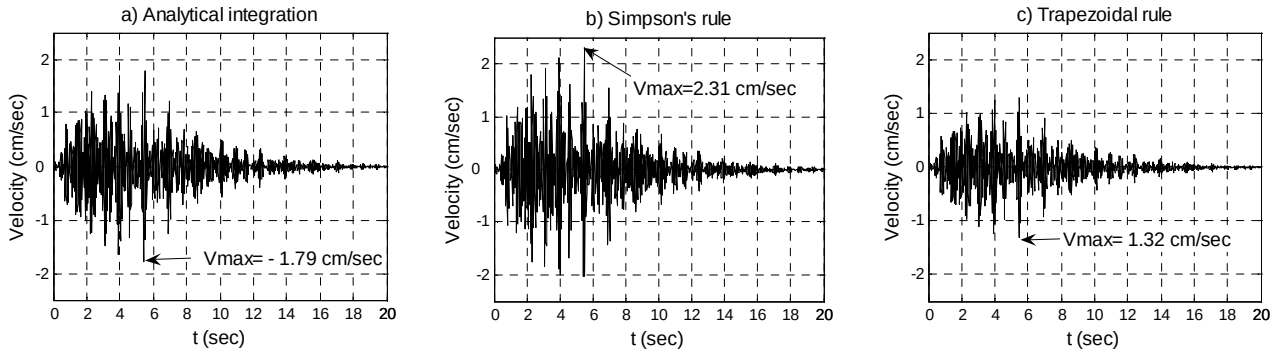

Figure 5.- Analytical a) vs. numerical integration [b) and c)] of the accelerogram shown in Fig. 4-b

As concerns the phase shift introduced by the rectangle rule, the apparent change of frequency of the integrated record associated to that shift translates into computational errors in engineering applications. As an example, Fig. 6 illustrates the results found applying the sliding block method (Newmark, 1965) to estimate the permanent seismic displacement of a gravity wall subjected to a single sine wave pulse of acceleration.

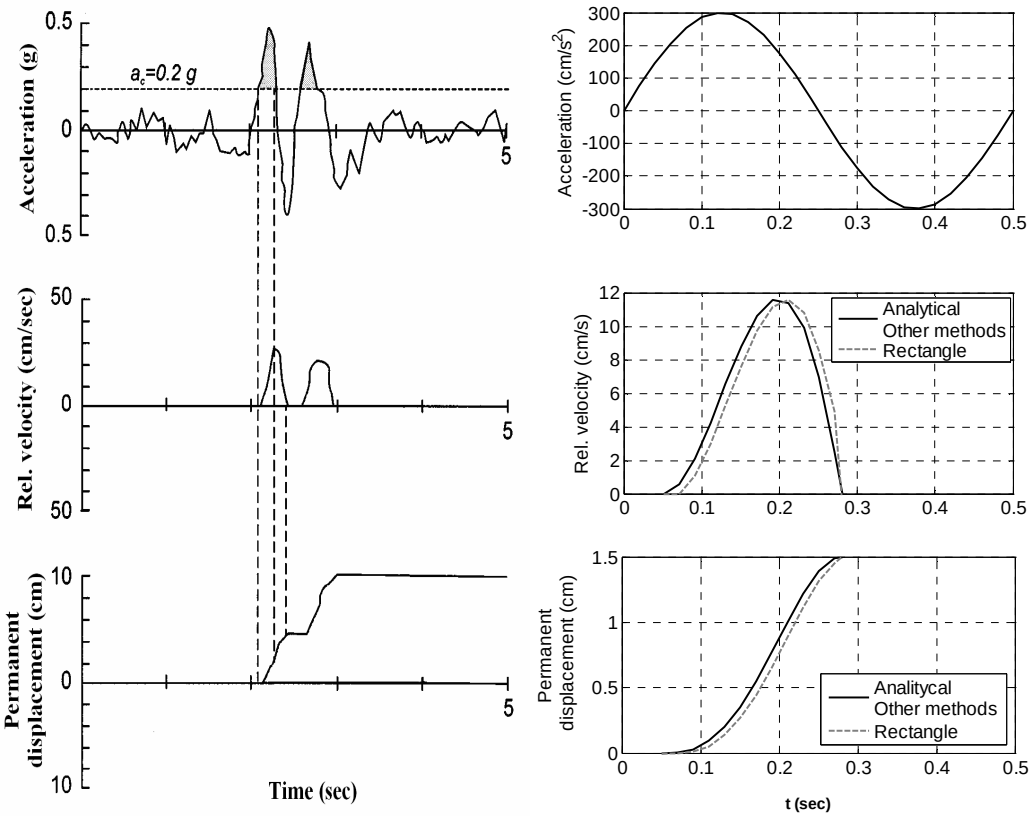

Figure 6.- Permanent seismic displacement of a gravity wall subjected to one cycle of harmonic acceleration; a) calculation procedure; b) numerical estimates using different quadrature rules.

3. ACCURACY OF NUMERICAL SEISMIC RESPONSE OF LINEAR SYSTEMS

3.1. Single-degree-of-freedom systems

The evaluation of the seismic response of a single-degree-of-freedom (S.D.O.F.) system subjected to an input base acceleration, $\ddot{y}(t)$, requires to solve the classical second-order ordinary differential equation

$$\ddot{u} + 2\xi p\dot{u} + p^2 u = -\ddot{y}(t) \qquad (3.13)$$

where $p=2\pi/T_n$ is the natural frequency of the oscillator, ξ is the damping ratio, and $u, \dot{u}, \ddot{u}$ stand for the relative displacement, relative velocity, and relative acceleration of the vibrating system.

Then, the dynamic response of the S.D.O.F. system can be written as:

$$u(t) = u_t(t) + u_f(t) \qquad (3.14)$$

u_t and u_f represent, respectively, the forced and free vibration phases of the motion, given by the relations (Veletsos and Ventura, 1985):

$$u_t(t) = -\int_0^t \ddot{y}(\tau) h(t-\tau) d\tau \qquad (3.15)$$

$$u_f(t) = U_0 \cdot g(t) + \dot{U}_0 \cdot h(t) \qquad (3.16)$$

and g(t) and h(t) are the so-called unit-response functions of the system

$$g(t) = \left[\cos(p_d t) + \frac{\xi}{\sqrt{1-\xi^2}} \sin(p_d t) \right] e^{-\xi p t} \qquad (3.17\text{-a})$$

$$h(t) = \frac{1}{p_d} e^{-\xi p t} \sin(p_d t) \qquad (3.17\text{-b})$$

In Eqs. 3.16 and 3.17, $p_d = p\sqrt{1-\xi^2}$, and $U_0, \dot{U}_0$ are, respectively, the initial displacement and the initial velocity of the system. For an oscillator initially "at rest", $U_0 = \dot{U}_0 = 0$, and $u(t) \equiv u_t(t)$. Under these conditions, two possible methods have been proposed in the literature for solving Eqn. 3.13 in the time domain:

- Direct integration of the differential equation (3.13), by numerical calculation of the so-called convolution integral or Duhamel's integral

$$u\ (t) = -\frac{1}{p_d} \int_0^t \ddot{y}(\tau) e^{-\xi p(t-\tau)} \sin[p_d (t-\tau)] d\tau \qquad (3.18)$$

- Step-by-step integration of Eqn 3.13, following a matricial marching scheme of the type

$$\begin{Bmatrix} u_{n+1} \\ \dot{u}_{n+1} \end{Bmatrix} = A(p,\xi) \begin{Bmatrix} u_n \\ \dot{u}_n \end{Bmatrix} + B(p,\xi) \begin{Bmatrix} \ddot{y}_n \\ \ddot{y}_{n+1} \end{Bmatrix} \qquad (3.19)$$

In both cases, the accuracy analysis is based in the comparison between the numerical transfer functions of u and $\dot{u}$ and the corresponding values for the exact integration of Eqn. 3.13. It must be remarked that this procedure differs substantially from the classical error analysis based on the amplitude decay and period elongation of the free response of the undamped system to an initial displacement (Humar,1990). Such an analysis considers only the matrix A (which controls the stability of the method), and does not take into account the forced terms of Eqn. 3.19 (Preumont, 1982).

3.1.1 Transfer functions

The transfer functions of a linear system are frequency operators which characterize the ratio between the kinematic responses of the system and the corresponding excitations in the frequency domain. The accuracy of these complex-variable functions depends largely on the numerical method used to calculate the response of the system, as it is shown next.

a) Exact transfer functions

Substituting in Eqn. 3.13: $\ddot{y}(t) = e^{i\omega t};\ u(t) = H_u^*(i\omega)e^{i\omega t};\ \dot{u}(t) = H_{\dot{u}}^*(i\omega)e^{i\omega t} = i\omega H_u^*(i\omega)e^{i\omega t};$ $\ddot{u}(t) = -\omega^2 H_u^*(i\omega)e^{i\omega t}$, the following expressions for the stationary response are found

$$H_u^*(i\omega) = \frac{1}{\omega^2 - p^2 - 2i\xi\omega p} \qquad (3.20)$$

$$H_{\dot{u}}^*(i\omega) = i\omega H_u^*(i\omega\xi) \qquad (3.21)$$

$$H_{\ddot{x}}^*(i\omega) = -2\xi p H_{\dot{u}}^*(i\omega) - p^2 H_u^*(i\omega) \qquad (3.22)$$

where $\ddot{x}(t) = \ddot{u}(t) + \ddot{y}(t)$ denotes the absolute acceleration of the oscillator. The moduli of the above functions are plotted in Fig. 7 for a short period oscillator (T_n= 0.1 sec.) with two different damping ratios. The phase diagrams of the same functions are shown in Fig. 8. It can be verified that increasing the level of damping, reduces significantly the peak response of the oscillator, but the overall behavior outside the band of resonance is not affected too much.

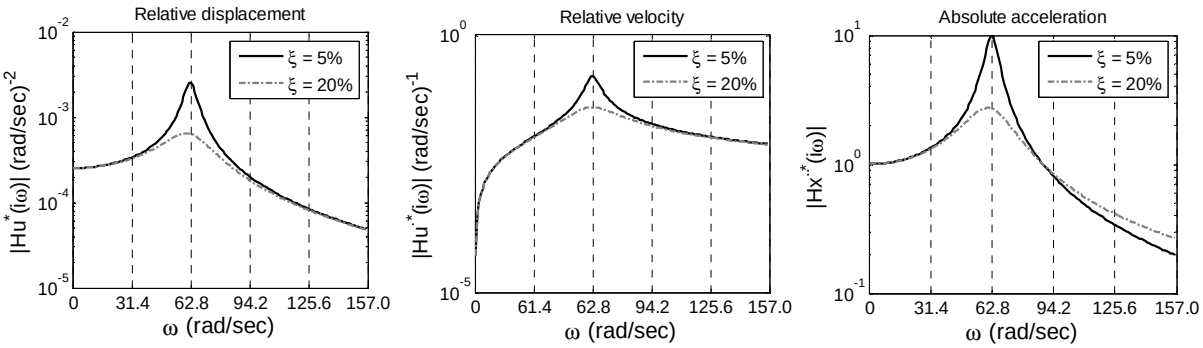

Figure 7.- Moduli of the exact transfer functions of short period oscillator (T_n=0.1 sec).

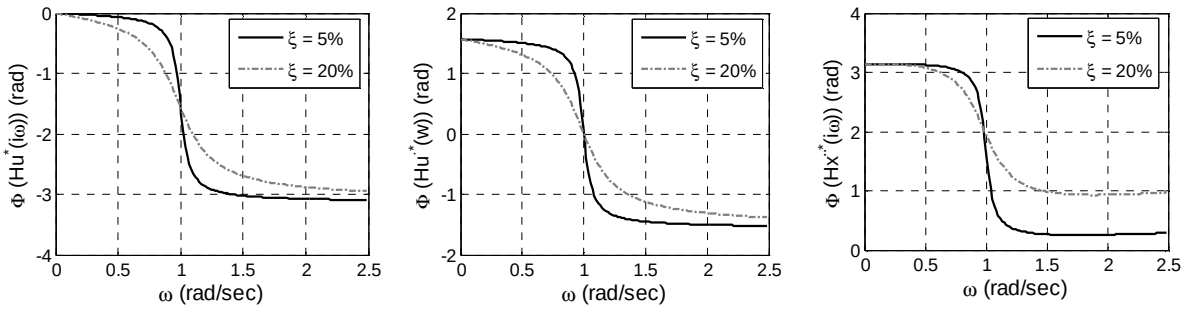

Figure 8.- Phase diagrams of the exact transfer functions of short-period oscillator (T_n=0.1 sec.)

b) Numerical transfer functions: Duhamel's approach

In this method the numerical errors are due solely to the amplitude of the integration interval, h (assumed in this work identical to the digitization interval), and/or the hypothesis made about the variation of the excitation, $\ddot{y}(t)$, between sampling points (Blázquez and Arcos, 1999a). In all cases the transfer functions will be limited to the uppermost value of the frequency: $\omega_N = \pi / h$ (Nyquist frequency) to prevent "aliasing phenomena".

Then, for a resting system, substituting in Eqn. 3.13 $\ddot{y}(\tau) = e^{i\omega\tau}$, and developing the integral, gives

$$u(t) = e^{-pt\xi}\left\{\frac{-\sin(p_d t)}{p_d}\int_0^t e^{i\omega\tau}e^{p\xi\tau}\cos(p_d\tau)d\tau + \frac{\cos(p_d t)}{p_d}\int_0^t e^{i\omega\tau}e^{p\xi\tau}\sin(p_d\tau)d\tau\right\} \qquad (3.23)$$

$$u(t) = \left\{\frac{e^{-pt\xi}}{p_d}[-H_1(i\omega,t)\cdot\sin(p_d t) + H_2(i\omega,t)\cdot\cos(p_d,t)]\right\}e^{i\omega t} = H_u(i\omega,t)e^{i\omega t} \qquad (3.24)$$

The time-dependent complex functions $H_1(i\omega,t)$ and $H_2(i\omega,t)$ represent, for each integration rule, the transfer functions associated to the respective integrals (sine or cosine) in Eqn. 3.23. These functions are evaluated using the rule of integration by parts:

$$v = \int e^{i\omega\tau}d\tau = H(i\omega)e^{i\omega\tau} \qquad (3.25)$$

where H(iω) are the functions defined in Eqn. 2.8 to 2.11. After some mathematical manipulations, it results:

$$H_1(i\omega,t) = \frac{H(i\omega)}{R^2+S^2}\left\{e^{pt\xi}[R\cdot\cos(p_d t) + S\cdot\sin(p_d t)] - \frac{R}{e^{i\omega t}}\right\} \qquad (3.26\text{-a})$$

$$H_2(i\omega,t) = \frac{-H(i\omega)}{R^2+S^2}\left\{e^{pt\xi}[S\cdot\cos(p_d t) - R\cdot\sin(p_d t)] - \frac{S}{e^{i\omega t}}\right\} \qquad (3.26\text{-b})$$

where $R = 1 + \xi pH(i\omega);\ S = p_d H(i\omega)$ (3.27)

Substituting Eqs. 3.26 in Eqn. 3.24, yields:

$$H_u(i\omega,t) = \frac{H^2(i\omega)}{1 + 2\xi pH(i\omega) + p^2H^2(i\omega)}\left[1 - e^{-(p\xi+i\omega)t}\left(\cos(p_d t) + \frac{1+\xi pH(i\omega)}{p_d H(i\omega)}\sin(p_d t)\right)\right] \qquad (3.28)$$

A similar expression has been derived by Lin (1967), for the stochastic response of a linear system to a weakly stationary random excitation, using a completely different approach. Note that $H_u(i\omega,t)$ is a non-stationary transfer function whose amplitude evolves with time, according to the transient nature of the seismic action (Fig. 9). As expected, when $t \rightarrow \infty$ the expression in brackets in Eqn 3.28 tends to unity, meaning that the stationary vibration phase has been reached. Under these conditions, substituting for example $H(i\omega)$ by $H^*(i\omega)$ in Eqn 3.28, the value of the exact transfer function of u(t) for the analytical integration, $H_u^*(i\omega)$, is obtained. This procedure applies to any integration rule used in conjunction with Eqn 3.28. Figs. 10-a and 10-b exemplify this methodology for the Duhamel-trapezoidal and Duhamel-Simpson methods applied to two 5% damped oscillators with natural periods 0.1 and 5 sec. It can be seen in the figure that the opposite amplification trends of the two quadrature rules (Fig 3-a) mark the behavior of the respective transfer functions outside the resonance band of the system.

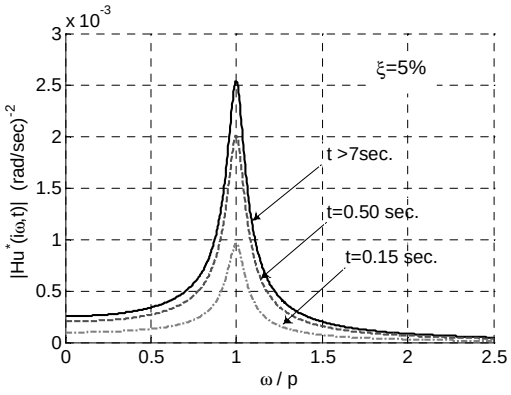

Figure 9.- Evolutionary transfer function amplitudes of the relative displacement of a 1 D.O.F. system at the transient (t < 7sec) and stationary (t ≥7sec) phases.

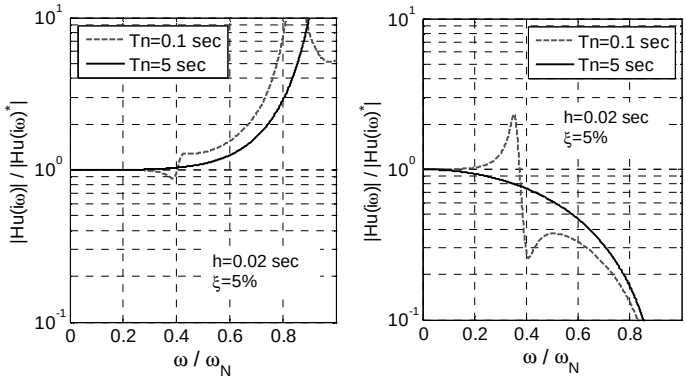

a) b)

Figure 10.- Normalized displacement transfer function diagrams for a 5%-damped system: a) Duhamel–Simpson rule, b) Duhamel-trapezoidal rule.

c) Numerical transfer functions: step-by-step integration algorithms

The way to proceed using this approach (Blázquez and Arcos, 1999b) is to derive the functions $H_u(i\omega,h), H_{\dot{u}}(i\omega,h)$, else solving the matricial Eqn. 3.19 as follows (n=number of sampled input values; I=unity matrix)

$$u_n = H_u(i\omega,h)e^{i\omega nh};\quad \dot{u}_n = H_{\dot{u}}(i\omega,h)e^{i\omega nh} \tag{3.29}$$

$$\begin{Bmatrix} H_u(i\omega,h) \\ H_{\dot{u}}(i\omega,h) \end{Bmatrix} = \left[e^{i\omega nh}I - A(p,\xi)\right]^{-1} B(p,\xi)\begin{Bmatrix} 1 \\ e^{iwnh} \end{Bmatrix} \tag{3.30}$$

or directly, from the mathematical scheme which defines the integration algorithm. For example, for the central difference method (explicit Newmark γ=1/2; β=0 method),

$$\dot{u}_n = \frac{1}{2h}(u_{n+1} - u_{n-1});\quad \ddot{u}_n = \frac{u_{n+1} - 2u_n + u_{n-1}}{h^2} \tag{3.31}$$

substituting in Eqn. 3.31, written in discrete form, the quantities: $u_n = H_u e^{i\omega nh}$; $u_{n-1} = H_u e^{i\omega(n-1)h}$; $u_{n+1} = H_u e^{i\omega(n+1)h}$; $\ddot{y}_n = e^{i\omega nh}$, it results

$$H_u(i\omega,h) = \frac{1}{2 - p^2 - 2\left(\cos(\omega h) + i\frac{\xi p}{h}\sin(\omega h)\right)} \tag{3.32}$$

which is the seismic transfer function of the method, strongly dependent on the amplitude of the integration interval, h. Note that while Eqs 3.32 applies only to steady-state conditions – that is when the transient phase of the forced vibration response has vanished – Eqn. 3.28 is valid for the transient and stationary phases, in spite of the fact that the latter is not always reached during seismic loading. Note also that, for the operators H_u and $H_{\dot{u}}$ being applicable in practice, they must comply with the consistency conditions

$$H_u(0) = H_u^*(0);\quad H_{\dot{u}}(0) = i\omega H_{\dot{u}}^*(0) \tag{3.33}$$

as well as with the standard requirements of stability and convergence of the method.

In this research, the performance of fourteen time stepping methods has been investigated, including three Runge-Kutta methods (2nd, 3rd and 4th order), five Newmark γ=1/2 methods (β=0, β=1/4, β=1/6, β=1/8, and β=1/12), three modified Newmark methods (HHT, WBZ and CH), and the Nigam-Jennings, Wilson θ=1.4 and Houbolt methods. Fig. 11 shows the normalized transfer functions of the displacement, velocity and acceleration of short and long period damped oscillators calculated using three of the above methods, namely the Nigam-Jennings (N-J), Houbolt and central difference methods. It is realized from the figure that the N-J method behaves smoothly throughout the whole range of frequencies, deamplifying lightly the response to high and low frequencies for all types of oscillators. On the contrary the other two methods show a strong resonance peak for all kinematic responses, diverging significantly from the exact ones in that zone. Furthermore, Fig. 11 confirms that, whereas the central difference method amplifies dangerously the excitation frequencies higher than the natural frequency, Houbolt's method filters those frequencies, which are not accurately integrated and, consequently, damped out in the response. This "numerical damping" effect is inherent to several integration methods (e.g. Wilson θ method), and acts similarly to modal truncation in the frequency domain analysis of multi-degree-of-freedom systems, leading ultimately to attenuated spectral ordinates in the high frequency region. Nevertheless, in practical computations, the presence of numerical damping is convenient, since it helps to maintain the stability of the conditionally stable integration methods, by keeping the high mode response of multi-degree-of freedom systems out of the solution.

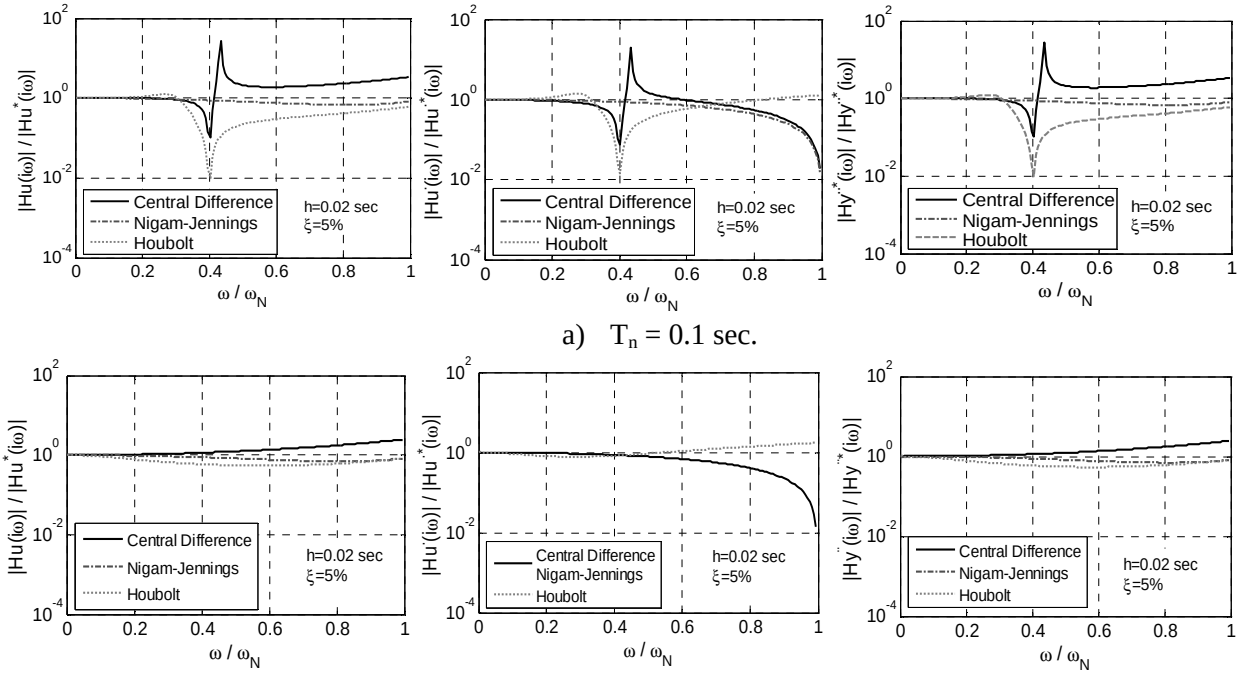

a) T_n = 0.1 sec.

b) T_n = 5 sec.

Figure 11.- Normalized Amplitude transfer function diagrams of three time stepping methods for short and long period S.D.O.F. systems.

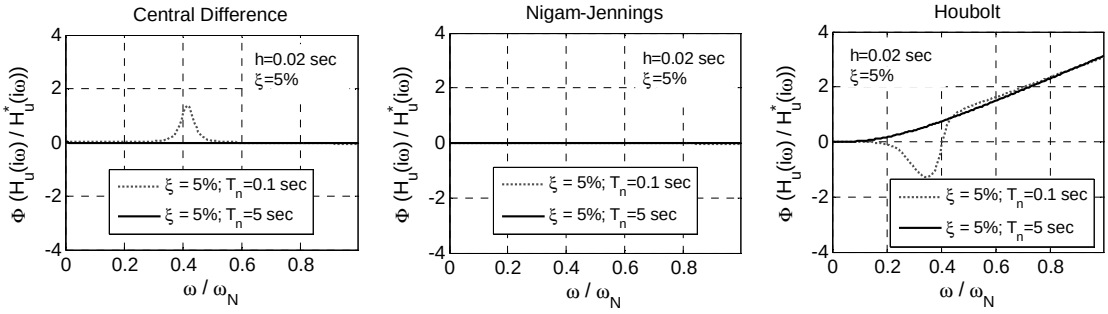

Figure 12.- Normalized displacement phase diagrams of three time stepping methods for short and long period S.D.O.F. systems.

Fig 12 visualizes the normalized phase angles of the N-J, Houbolt and central difference methods. Attention is brought to the fact that Houbolt's method introduces a marked distortion in the phase angles of the response, which become frequency-dependent. This feature is undesirable and may explain the poor accuracy of this method in solving certain dynamical problems

3.1.1 Response spectrum analysis

As explained before, all the integration schemes, even if they meet stability, convergence and consistency requirements, introduce numerical errors in the seismic response of S.D.O.F. systems, which result in misleading response spectra. Fig. 13-b displays the peak errors of the response relative to the analytical absolute acceleration spectrum of the input record shown in Fig. 4-a. It can be seen that the accuracy errors on the forced vibration phase affect basically to the low periods, and should not be confused with the amplitude decay errors reported elsewhere (Humar, 1990) for the free vibration phase, that affect basically to long period systems. It is also observed that the Nigam-Jennings method and the 3rd order Runge-Kutta method (Heun's method) provide very similar results (Fig. 13-a). The N-J method has proved to be more accurate and less costly in terms of computing time than the 3rd order Runge-Kutta method that was the standard for response spectra calculations prior to 1968.

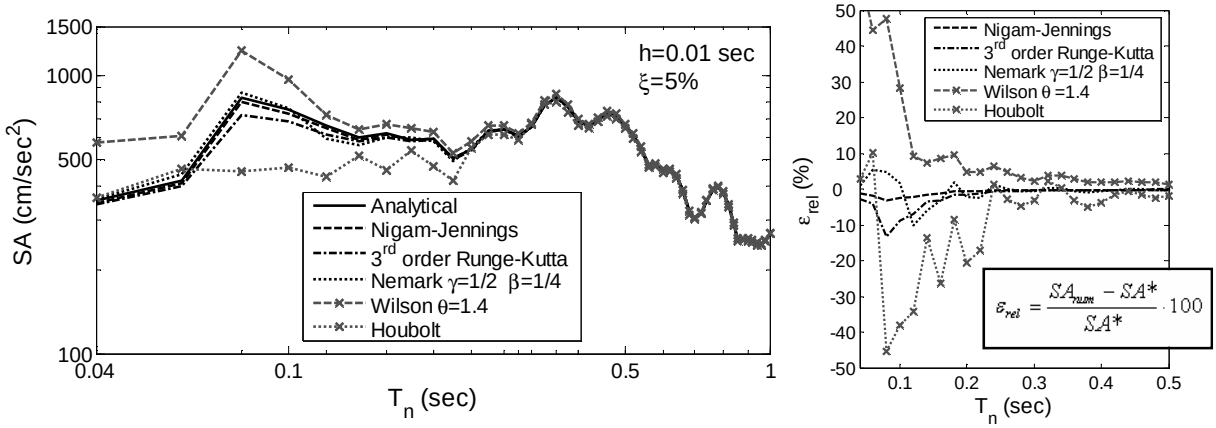

a) b)

Figure 13.- a) Numerical vs. analytical absolute acceleration spectra of the artificial accelerogram of Fig. 4-a; b) relative error of the numerical (approximate) spectrum ordinates with respect to the analytical (exact) values.

3.2. One-dimensional continuum systems

Continuum elastic systems have an infinite number of degrees of freedom (infinite number of natural frequencies) and therefore their seismic response is considerable more complex and difficult to obtain analytically than that of discrete systems, even in 1-D situations. To illustrate this point, consider the seismic response of the homogeneous elastic soil layer shown in Fig. 13, which rests on a rigid rock base. Assuming that the soil and bedrock extend infinitely in the lateral direction, the relative horizontal displacement, $u_r(t)$, at any point in the sand layer has been reported by Idriss and Seed (1968) as

$$u_r(t) = -\sum_{n=1}^{\infty} Y_n(y) X_n(t) = -\sum_{n=1}^{\infty} \sqrt{\frac{z}{H}} \frac{J_{-1/2}(\beta_n z/H)}{J_{1/2}(\beta_n)} \int_0^t \ddot{y}(\tau) sen[\omega_n (t-\tau)] d\tau \qquad (3.34)$$

were $\beta_n = \frac{(2n-1)\pi}{2}$, $\omega_n = \frac{\beta_n v_s}{H}$ is the circular natural frequency of the nth mode of vibration, $v_s = \sqrt{G/\rho}$ is the velocity of the shear waves propagating vertically in the deposit, and $J_\alpha(\cdot)$ is the Bessel function of first kind of order α.

Eqn. 3.34 has been applied to the surface (point A) of a 30m-thick soil layer, with ρ=1920 Kg/m^3 and variable shear modulus, G (Fig. 14-a), subjected to a harmonic acceleration (in gal) at the bedrock of the type:

$$\ddot{y}(t) = 300 sen(2\pi t) + a^* sen(\omega^* \cdot t) \qquad (3.35)$$

where the pair of values (a*,ω*) represent the amplitude and circular frequency of a contaminating noise, either or low or high frequency (Fig. 14-b). With these premises, the numerical relative errors arisen when computing $u_r(t)$ (Eqn. 3.34) by means of the N-J and the Newmark β=1/4 algorithms are displayed in Fig. 14-c for different values of G. Two observations are made. First, only unconditionally stable methods can be used reliably in the determination of $u_r(t)$, since all other methods will not meet the stability requirements for high values of n in Eqn. 3.34, making the calculation to fail. Secondly, both methods damp out the system response to the high frequency noise, in agreement with the values of the parameter $|H_u(i\omega)/H_u^*(i\omega)|$ in that. This favorable effect is more dramatic for the Newmark-β=1/4 method than for the N-J method.

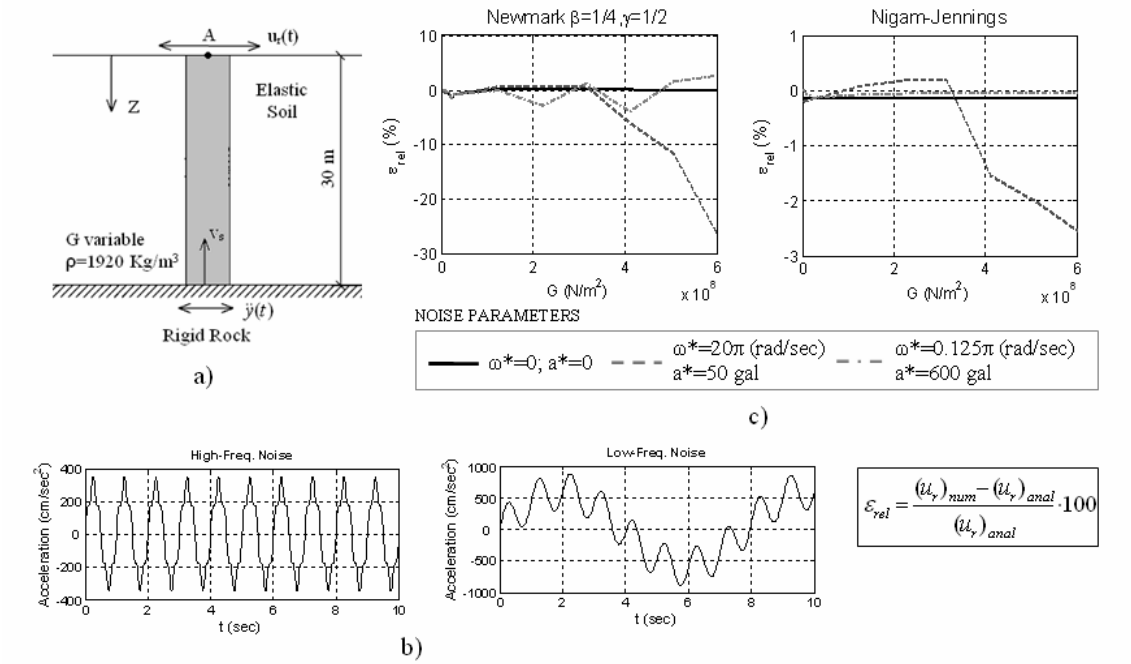

Figure 14.- Displacement response at top of uniform elastic soil layer (a) to clean and noise-contaminated accelerograms (b). Computational error of numerical methods (c).

4. EFFECT OF SYSTEM INITIAL CONDITONS ON ELASTIC RESPONSE SPECTRA

4.1. Theoretical background

Presently, elastic response spectrum plots are a standard design tool to characterize the frequency content of an earthquake and its effects on structures. They are obtained by maximizing the solution of the equation of motion of the S.D.O.F. system (Eqn. 3.13) as well as the related magnitudes (relative velocity and absolute acceleration of the oscillator), in the following manner:

$$SD = |u(t)|_{\max}; \quad SV = |\dot{u}(t)|_{\max}; \quad SA = |\ddot{x}(t)|_{\max} \qquad (4.36)$$

where SD, SV, and SA represent, respectively, the true relative displacement, relative velocity and absolute acceleration response spectra. If the damping ratio is low($\xi \rightarrow 0$), a quasi-linear behavior of the system can be assumed, and the true velocity and acceleration spectra can be substituted by the so-called pseudoresponse spectra, defined as

$$PSV = p \cdot SD = \frac{2\pi}{T} \cdot SD \approx SV \qquad (4.37\text{-a})$$

$$PSA = p^2 \cdot SD = \left(\frac{2\pi}{T}\right)^2 \cdot SD \approx SA \qquad (4.37\text{-b})$$

Eqs. 4.37 are highly sensitive to the variations of the parameters ξ and T (previously called T_n), specially for long-period systems. Fig 15 confirms that, for a oscillator initially at rest, with a period much higher than the period of the excitation, PSA≈SA for all periods, but PSV≈SV only for intermediate periods. For periods greater than a certain critical value ($T>T_{crit}$), the SV curve departs clearly from the PSV curve and approaches its asymptotic value, the maximum velocity of the ground, $|\dot{y}(t)|_{max}$. On the other hand, for the same conditions, $PSV = \frac{2\pi}{T} \cdot SD \to 0$, since SD approaches its limiting value, $|y(t)|_{max}$, while T increases indefinitely (Hudson, 1979). Then, it is concluded that, for long period systems, velocity and pseudo-velocity response spectra are not exchangeable, even in the case of very low damping.
Even more important is to recognize the effect of the initial system conditions in both, true and pseudoresponse spectra, for elastic long period systems, whose maximum response is very often attained after cessation of the excitation, during the first half-cycle of free vibration.

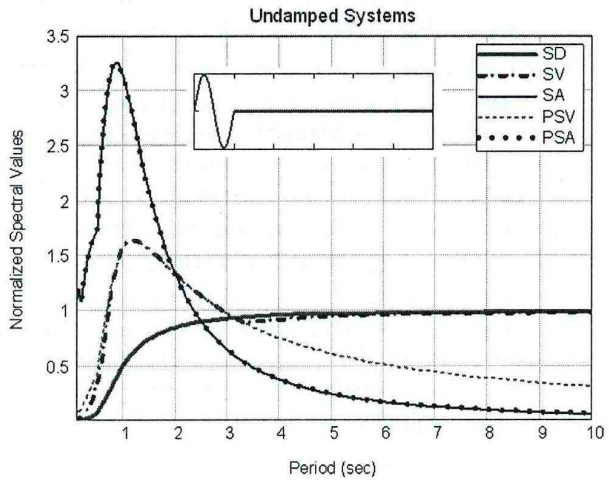

Figure 15.- True and pseudoresponse spectra for sine acceleration pulse.

Using a single cycle sinusoidal acceleration wave of period T_0 as excitation of a system of period T, Blázquez and Kelly (1988) have shown (Fig. 16) that, for short period rigid systems ($T \leq T_0$), the free vibration component in Eqn. 3.14 can be neglected and the effect of the initial conditions is negligible regardless of the damping level; thus it can be reasonably assumed that:

$$U_0 = u(0) \approx 0 \;;\; \dot{U}_0 = \dot{u}(0) \approx 0 \qquad (4.38\text{-a})$$

In contrast, for long period flexible systems ($T \geq T_0$), the following asymptotic relations can be used to approximate initial conditions:

$$U_0 = u(0) \approx -y_0 \;;\; \dot{U}_0 = \dot{u}(0) \approx -\dot{y}_0 \qquad (4.38\text{-b})$$

where y_0 and $\dot{y}_0$ are, respectively, the input displacement and the input velocity at the initial time of motion.

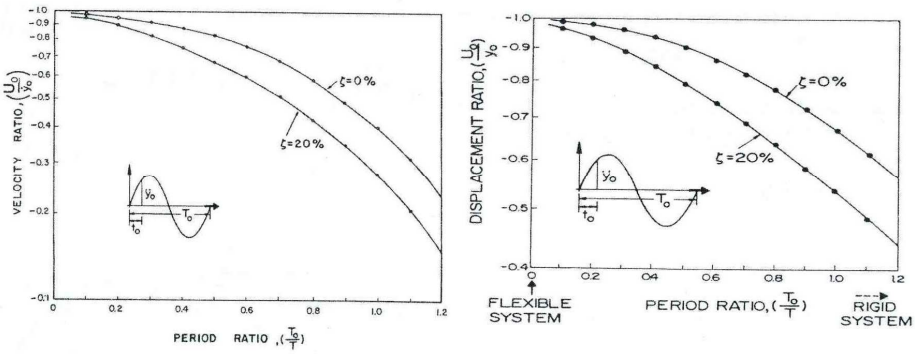

Figure 16.- Ratios of initial motions of a S.D.O.F. system to the initial motions of the ground for sinusoidal acceleration wave (Blázquez and Kelly, 1988)

Since the standard method for calculating response spectra assumes zero initial conditions, it is concluded that, strictly speaking, such a procedure applies only to high-frequency systems (e.g. rigid structures) with non-zero initial conditions. For other types of systems (particularly flexible ones), the effect of initial conditions on the long period regions of response spectra remains to be clarified.

4.2. Parametric study

To investigate the implications of considering or neglecting the effects of the initial conditions in the response spectrum analysis, a parametric study of the spectral responses of a viscously damped S.D.O.F elastic system has been conducted. To this end, the peak ground acceleration, $\ddot{Y}$, the initial conditions, U_0 and $\dot{U}_0$, and the natural frequency of the system, p, are interrelated by the dimensionless coefficients:

$$\alpha = -p^2 \cdot \frac{U_0}{\ddot{Y}} \quad ; \quad \beta = -p \cdot \frac{\dot{U}_0}{\ddot{Y}} \qquad (4.39)$$

and the sensitivity of the response to various combinations of α and β is evaluated for different types of excitations at the base of the system.

4.2.1 Sinusoidal pulse acceleration

For a single cycle of excitation of the form $\ddot{y} = \ddot{Y}\sin(2\pi t / T_0)$, in which T0 is the duration of the cycle, the normalized spectral displacement, *SD/Y*, spectral velocity, $SV/\dot{Y}$, pseudo-spectral velocity, $PSV/\dot{Y}$, and absolute spectral acceleration, $SA/\ddot{Y}$, of undamped systems, have been calculated by Ventura and Blázquez (1990, 1992), for different pairs of values of α and β. Fig. 17 shows a sample of the computed results as a function of the ratio T/T0. It can be seen that the broken lines in Fig. 17 exhibit a linear trend for large values of T/T0 in the case of the velocity spectra (SV and PSV), and a parabolic shape in the case of the displacement spectra (SD). The reason is that, for a harmonic pulse and fixed values of α and β, Eqs. 4.39 can be written

$$U_0 = -\frac{\ddot{Y}\alpha}{p^2} = -Y\alpha\left(\frac{T}{T_0}\right)^2 \qquad (4.40\text{-a})$$

$$\dot{U}_0 = -\frac{\ddot{Y}\beta}{p} = -\dot{Y}\beta\left(\frac{T}{T_0}\right) \qquad (4.40\text{-b})$$

and therefore the initial motions of the system, U_0 and $\dot{U}_0$ are much larger than the peak values of the base displacement, Y, and base velocity, $\dot{Y}$, respectively. Therefore, since the maximum response of the transient part (u_t in Eqs. 3.14 and 3.15) approaches *Y*, it becomes clear that the response is dominated by the free vibration part (u_f in Eqs. 3.14 and 3.16), as indicated in Fig. 17. In all cases the effect of damping is simply to reduce the amplitude of motion of the response of the system.

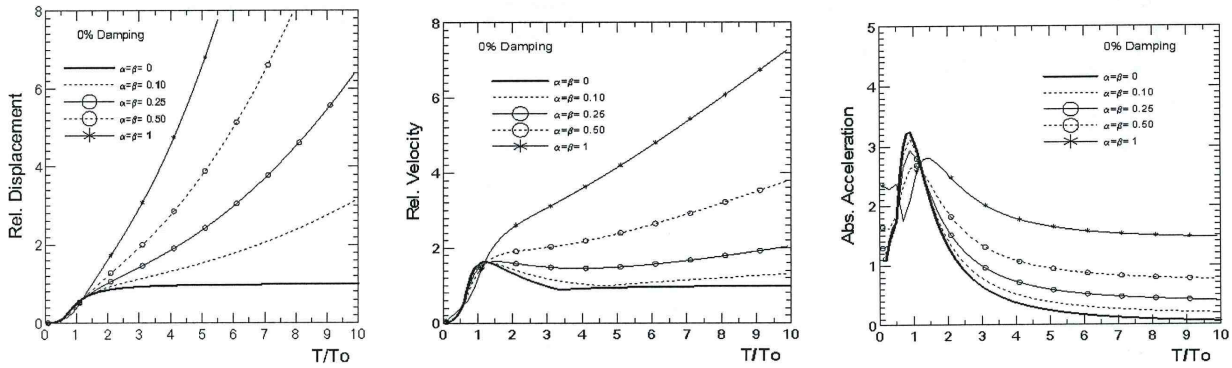

Figure 17.- Effect of initial conditions on the normalized spectra of undamped S.D.O.F. systems subjected to sinusoidal base acceleration (Ventura and Blázquez, 2007)

4.2.2 Earthquake input acceleration

For more complex excitations, such as real or artificially generated seismic motions, the same trends on the variation of the response spectra are found, as long as one of the values α and β, at least,is different from zero.
As an example, the response spectra for the 1940 El Centro earthquake record (N-S component) with and without initial conditions are shown in Fig. 18, and the spectra for the 1985 Mexico earthquake recorded at the SCT station (E-W component) are shown in Fig. 19. The El Centro earthquake has been selected because it produces significant responses over a wide band of system periods, while the Mexico earthquake produces significant responses for a narrow range of high periods, mostly between 1.5 and 3 sec.
Fig. 18 and 19 evidence that the effect of initial conditions on the response of rigid systems is quite negligible, since they are more sensitive to the high frequency components of the input motion than to the initial state of the system. On the contrary, the long period systems are much more influenced by the initial conditions on PSV and SA than any other type of systems. The SA spectra also show that the base shear for a long period system with non-zero initial conditions is larger than that for a system initially at rest. This fact may lead to unconservative designs of long period structures if the initial conditions effects are not properly accounted for.

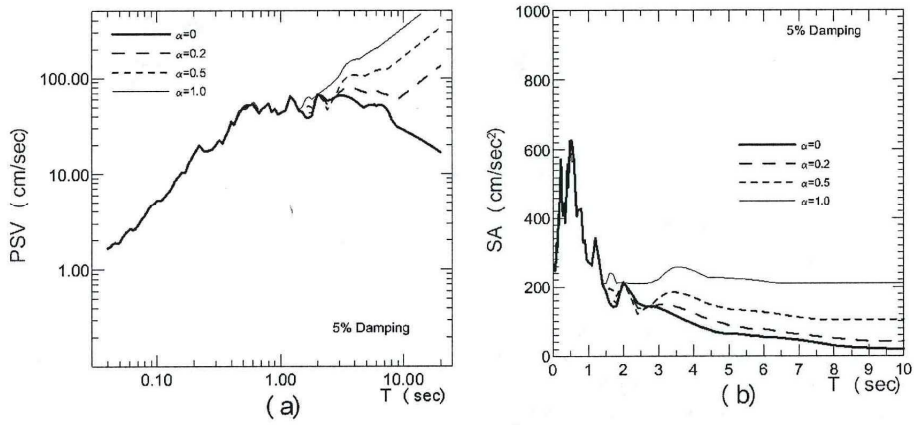

Figure 18.- Influence of initial displacement (α) on pseudo-velocity (PSV) and absolute acceleration (SA) response spectra for elastic systems subjected to El Centro 1940 earthquake, N-S component (Ventura and Blázquez, 2007)

4.3. Application to analog accelerograms

The results presented in the above sections are useful inasmuch as they provide the behavioral pattern of the initial conditions problem. However they are difficult to link to the primary cause of $u(0)$ and/or $\dot{u}(0)$ being nonzero, which is usually the lost initial part of the analog accelerograms that leads to assuming arbitrarily that

the unknown motions at zero time (when the instrument is triggered) are $U_0 = u(0) = 0;\ \dot{U}_0 = \dot{u}(0) = 0$. To cope with this problem, the pretriggering event for a strong motion record has been simulated herein by artificially cutting off a prefixed segment of the record, t_0 (corresponding to a trigger acceleration a_t), so that the response spectra of the truncated and untruncated input motions can be compared.

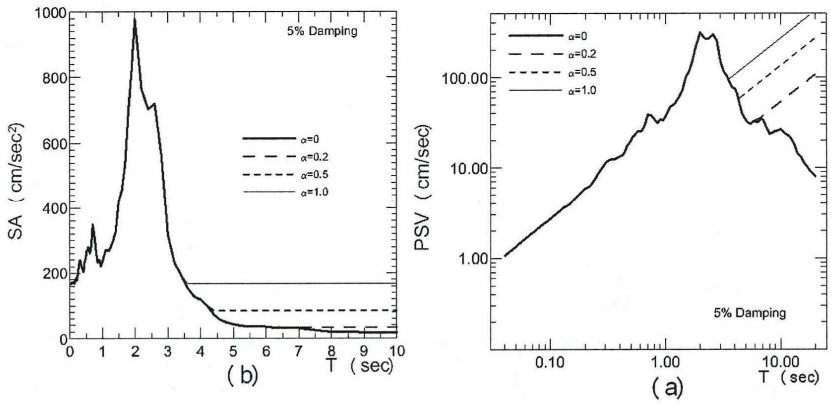

Figure 19.- Influence of initial displacement (α) on pseudo-velocity (PSV) and absolute acceleration (SA) response spectra for elastic systems subjected to Mexico 1985 earthquake, E-W component (Ventura and Blázquez, 2007)

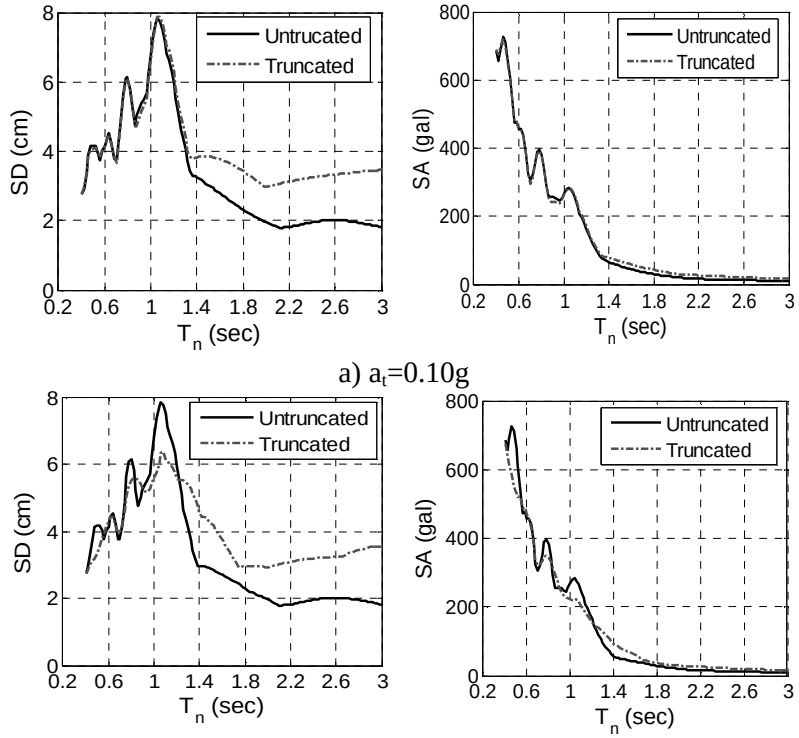

Figure 20.- Spectral behaviour of truncated and untruncated analog accelerograms (Fig. 4-a; a_{max}=0.33g) for a trigger acceleration: a) a_t=0.10g ; b) a_t=0.20g (instrument malfunction).

This procedure has been applied to an artificial earthquake with analytically amenable response spectra, thereof permitting a direct comparison between the observed and ideal measurements, with no numerical errors whatsoever in the computational process. The results of such a comparison, for the artificial accelerogram of Fig. 4-a, are given in Fig. 20, considering either an untruncated (complete) record with $U_0 \neq 0$ and/or $\dot{U}_0 \neq 0$

at t=t_0 or a truncated (incomplete) record with $U_0 = \dot{U}_0 = 0$ at t=t_0. In the last case U_0 and $\dot{U}_0$ are unknown and therefore, in common practice, they are both assume to be zero in spectral calculations. The diagrams show in Fig. 20 point out, that, at the long period range, the SA values are almost insensitive to the truncation of the accelerogram, whereas the SD values of the incomplete records are consistently higher than the SD values of the complete records. Moreover, for very high periods, the undamped PSV spectrum of incomplete records tends asymptotically to the peak ground velocity instead to zero (Blázquez and Kelly, 1988; Pecknold and Riddell, 1978; Fig. 21).

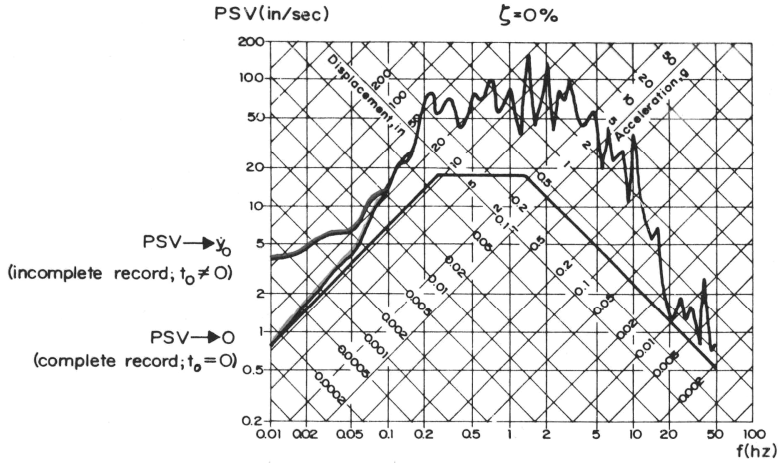

Figure 21.- Asymptotic behaviour of incomplete analog accelerograms at long periods (Pecknold and Riddell, 1978).

4. CONCLUSIONS

1) Algorithms that amplify significantly the upper half part of the Nyquist interval are very sensitive to the presence of spurious high frequency noise in seismic signals and should be avoided in dynamic response computations.

2) Phase shift in integration schemes distorts the frequency content and the shape of the excitation signals, introducing unacceptable drift errors in the integrated records.

3) The amplitude of the integration interval is the main parameter controlling the stability and accuracy of seismic response of linear systems: the smaller the interval the greater the accuracy.

4) In general, numerical transfer functions of S.D.O.F. systems (especially short period systems) show a sharp peak at the resonance region of the oscillator, diverging considerably from the shape of the exact transfer curves in that zone.

5) Time-dependent Duhamel's transfer functions apply to the transient and stationary phases of the evolutionary seismic motions, while for step-by-step methods only the transfer functions of the stationary phases are computed.

6) Integration methods that introduce numerical damping in the response of the system filter out the high frequencies from the system's response. The truncation effect is very smooth and uniform for Nigam-Jennings method which deamplifies lightly the whole range of frequencies for all types of oscillators.

7) For long period (flexible) systems, the effect of non-zero initial conditions in the motion is a magnification of the spectral values, regardless of the damping level of the system. These values are dominated by the free vibration part of the response of the system.

8) For short to intermediate period systems (rigid) the above effect is quite negligible, since they are more sensitive to the high frequency components of the input motion than to the initial state of the system.

9) The base shear for a long period elastic system with non-zero initial conditions may be significantly larger than for a system initially at rest, leading to an unconservative design if this effect is not properly accounted for.

10) Omitting initial conditions makes the pseudo-velocity spectrum to deviate from zero at very long periods and asymptotically approach the initial absolute velocity of the system.

REFERENCES

Blázquez, R. and Arcos, A. (1999a). Numerical errors in the computation of Duhamel's integral. 2éme Rencontre en Génie Parasismique des Pays Méditerranéens (SISMICA 99), Faro, Portugal, 435-444.

Blázquez, R. and Arcos, A. (1999b). Transfer functions of time integration algorithms used in response spectrum analysis of earthquakes. Proceedings of the Fourth European Conference on Structural Dynamics (EURODYN'99), Prague, Czech Republic, 7-10 June, 1087-1093.

Blázquez, R. and Kelly, J.M. (1988), Effect of initial conditions and computational algorithm on long period response spectra, IX World Conference on Earthquake Engineering, Tokyo-Kyoto, Japan, **5**, 1051-1056.

Bogdanoff, J.L., Godberg, J.E. and Bernard, M.C. (1961). Response of a simple structure to a random earthquake type disturbance. Bulletin of the Seismological Society of America, **51:2**, 293-310.

Hamming, R.W. (1977). Digital filters. Prentice-Hall International, Inc., Englewood Cliffs, N.J.

Humar, J.L. (1990). Dynamics of Structures. PrenticeHall, Englewood Cliffs, N.J.

Hudson, D.E. (1979). Reading and interpreting strong motion accelerograms. EERI Monograph, Berkeley, CA.

Idriss, I.M. and Seed, H.B. (1968). Seismic response of horizontal soil layers. Journal of the Soil Mechanics and Foundations Division, American Society of Civil Engineers, **94:SM4**, 1003-14031.

Lin, Y.K. (1967). Probabilistic theory of structural dynamics. Mc Graw-Hill, Inc., New York.

Newmark, N. (1965), Effects of earthquakes on dams and embankments. Geotechnique, **15:2**, 139-160.

Pecknold, D.A., and Ridell, R. (1978). Effect of initial base motion on response spectra. Engineering Mechanics, ASCE, **104-EM2**, 485-491.

Preumont, A. (1982). Frequency domain analysis of time integration operators. Earthquake Engineering and Structural Dynamics, **10**, 691-697.

Veletsos, A.S. and Ventura, C.E. (1985). Dynamic analysis of structures by the DFT Method. Structural Engineering, ASCE, **III:12**, 2625-2642.

Ventura, C. and Blázquez, R. (2007). Effect of system initial conditions on seismic design of long-period structures. ISET Journal of Earthquake Technology, **1**, 111-126.